Theor Chem Acc (2013) 132:1338
DOI 10.1007/s00214-013-1338-8

REGULAR ARTICLE

MS-CASPT2 study of the low-lying electronic excited states of di-thiosubstituted formic acid dimers

R. Verzeni · O. Mó · A. Cimas · I. Corral · M. Yáñez

Received: 31 October 2012 / Accepted: 6 January 2013 / Published online: 30 January 2013

Abstract The suitability of di-thiosubstituted derivatives of formic acid dimer, both in hydroxyl and carbonyl position, as possible hydrogen-bonded electron transfer linkers in a hypothetical donor–acceptor dyad for photovoltaic cells and artificial photosynthesis reactors has been studied from a theoretical point of view. To this purpose, the valence singlet electronic excited states of the four possible di-thiosubstituted isomers have been characterized through multi-state complete active space second-order perturbation theory (MS-CASPT2). These hydrogen-bonded systems present electronic spectra consisting of nπ* and ππ* excitations, both intra- and intermonomer. The eventual comparison of the calculated spectroscopic characteristics of the isolated hydrogen-bonded linkers with the experimental spectrum of the chromophore in a donor–acceptor dyad could allow establishing whether the linker would compete with the electron donor in the photon absorption process. Additionally, the analysis of the structural changes undergone by these species upon electronic excitation to the S_1 would allow determining whether the population of this state of the linker upon UV–vis light absorption could compromise the formation of the charge transfer complex, key in the performance of photovoltaic devices.

Keywords Hydrogen-bonded linkers · Formic acid dimer · Di-thiosubstituted derivatives · MS-CASPT2 · Solar cells · Charge transfer · Donor–acceptor dyad

Published as part of the special collection of articles derived from the 8th Congress on Electronic Structure: Principles and Applications (ESPA 2012).

This paper is dedicated to Prof. Ria Broer, a good scientist and a better friend, on occasion of her 60th birthday.

R. Verzeni · O. Mó · I. Corral (✉) · M. Yáñez
Departamento de Química, Facultad de Ciencias, Universidad Autónoma de Madrid, Cantoblanco, 28049 Madrid, Spain
e-mail: ines.corral@uam.es

A. Cimas
Centro de Investigação em Química, Department of Chemistry and Biochemistry, Faculty of Science, University of Porto, Rua do Campo Alegre, 687, 4169-007 Porto, Portugal

1 Introduction

In the last decades, the increasing demand of new materials and electronic nanodevices for high-performance organic solar cells [1–5] has motivated a growing interest on solar energy convertors based on the same key process, a photoexcitation leading to a charge separation [1, 5]. The simplest version of such photovoltaic devices is a donor–acceptor dyad at least composed by an electron donor chromophore, an electron acceptor and a linker that controls their distance and electronic interactions. In an organic photovoltaic cell, the dyad is connected to two electrodes, which convey the two-formed charges in a circuit, producing electrical current.

The process of charge separation starts when a photon hits the chromophore, generating an exciton. Under normal conditions, the exciton does not travel long distances, and the chromophore remains in the so-called excited state that usually decays rapidly, relaxing either radiatively or thermally. Nevertheless, under certain circumstances, the above relaxation mechanisms compete with other processes such as charge transfer (CT), for instance in those cases where the chromophore is connected to a strong electron acceptor. In these situations, the exciton could be forced to dissociate driving the system into a CT complex,

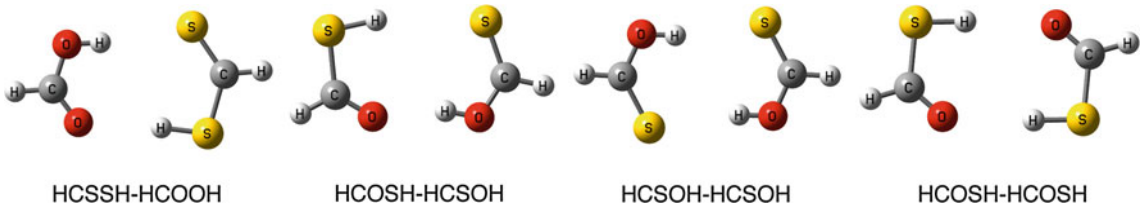

Fig. 1 Formic acid dimer di-thiosubstituted derivatives

where the electron has been transferred to one of the acceptor's lowest lying unoccupied MOs (LUMOs) and the hole still remains on one of the donor highest lying occupied MOs (HOMOs). This hybrid state, lying at the interface between donor and acceptor moieties, governs in solar cells both the voltage-dependent photocurrent as well as the open circuit voltage [5]. The efficiency and the rate of this final step depend on macroscopic values as charge carriers' average mobility, materials' average dielectric constant, and distance below which the CT complex polarons thermally relax, [5, 6] but also on microscopic aspects such as coulombic interactions caused by molecules orientation toward the heterojunction [5, 7].

Inspired by the efficiency of biological photosynthesis, the number of biomimetic studies on the control of electron transfer reactions through a network of hydrogen bonds (HBs) has significantly increased [4, 8]. Indeed, it has been shown that hydrogen-bonded donor–acceptor assemblies ensure more efficient electronic communication than comparable σ- or π-bonding networks [9, 10].

However, in the event that the electronic absorption spectra of the hydrogen-bonded connector and that of the electron donor overlap, the efficiency of the entire device can be seriously compromised, directly, due to the reduction in potentially absorbable photons by the electron donor, preventing the formation of excitons, or indirectly, since geometric changes in the hydrogen-bonded linker, due to its electronic excitation, could interfere with the formation of the CT complex and/or its dissociation, ultimately provoking a collapse of the hydrogen-bonded photovoltaic device. Therefore, the spectroscopic characterization of the connector is of fundamental importance for the successful design of a charge separation reaction center. The aim of this paper is to present such a spectroscopic characterization for the linkers built-up from the substitution of two oxygen atoms in formic acid dimer and leading to the four hydrogen-bonded complexes: HCSSH–HCOOH, HCOSH–HCSOH, HCSOH–HCSOH, and HCOSH–HCOSH, shown in Fig. 1. Similar species based on double HB interactions between a carboxylate anion and an amidinium cation have been used in dyads with photovoltaic activity. The comparison of the results for the di-thiosubstituted dimers with those obtained for formic acid dimer and its mono-thiosubstituted derivatives will allow determining the effect that a second sulfur atom has in the UV absorption spectra of these systems and whether their spectroscopic properties could broaden the range of chromophores with which the new linkers can be used.

Finally, the characterization of the structure and bonding of the first electronic excited state in these systems will allow estimating the impact that, in the CT complex of the photovoltaic device, has the change in the structure of the linker in the hypothetical case, these electronic states are populated by UV–vis photons.

To our knowledge, no experimental spectroscopic studies on formic acid dimer di-thiosubstituted derivatives have been reported to date (Table 1).

Table 1 Summary of formic acid dimer and its monosubstituted derivatives vertical energies and oscillator strengths for the electronic transitions absorbing below 10 eV, analyzed in Ref. [27]

	HCOOH–HCOOH		HCOSH–HCOOH		HCSOH–HCOOH	
	ΔE/eV	f	ΔE/eV	f	ΔE/eV	f
Intra-monomer						
$n_{c=o}\pi^*_{c=o}$	6.13	0.000	6.17	0.001	6.27	0.001
$n_{c=x}\pi^*_{c=x}$(S)	6.21	0.001	4.94	0.000	3.82	0.000
$\pi_{c=o}\pi^*_{c=o}$	8.25	0.655	8.31	0.456	8.33	0.471
$\pi_{c=x}\pi^*_{c=x}$(S)	7.56[a]	0.000	5.98	0.396	5.58	0.477
Inter-monomer						
$n_{c=x}\pi^*_{c=x}$	9.13	0.002	8.71	0.000	8.92	0.001
$n_{c=x}\pi^*_{c=x}$(S)	9.17	0.000	10.63	0.000	8.62	0.002
$\pi_{c=x}\pi^*_{c=x}$	9.80	0.000	9.59	0.004	9.84	0.035
$\pi_{c=x}\pi^*_{c=x}$(S)	9.93	0.005	9.71	0.011	8.73	0.003

(S) only applies to HCOSH–HCOOH and HCSOH–HCOOH dimers and denotes, in the intramonomer section, transitions occurring in the thiosubstituted monomer and, in the intermonomer section, transitions where the electron is promoted from an orbital from the thiosubstituted monomer

[a] Excitation energy underestimated due to the very low reference weight in the CASPT2 calculation. This transition is expected to peak at 8.25 eV [27]

2 Computational details

The ground state structures of the four studied dimers were optimized using the B3LYP [11, 12] functional in

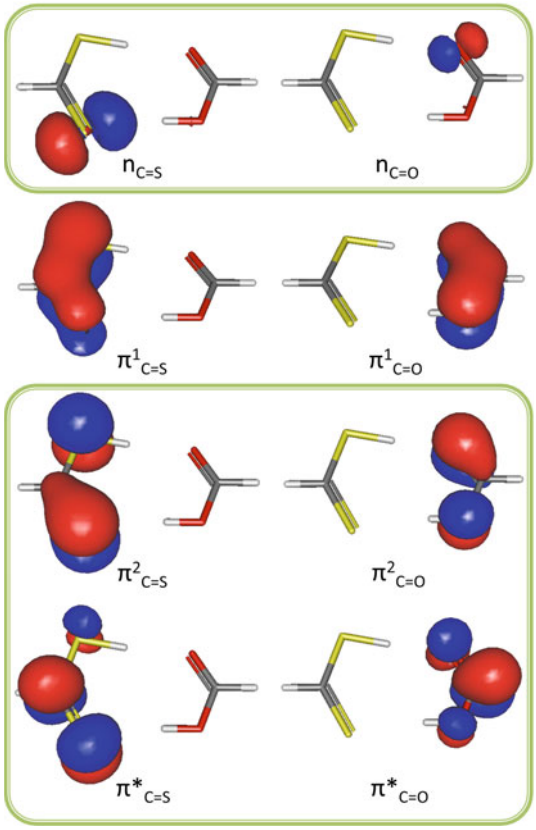

Fig. 2 Exemplary SA-CASSCF valence molecular orbitals used in the calculation of A′ and A″ electronic transitions of the HCSSH–HCOOH dimer. Sulfur and oxygen atoms are represented in *yellow* and *red*, respectively. The n superindex of π^n orbitals denotes the total number of nodes of the MO. Similar orbitals or linear combinations of them were obtained in the excited state calculations of the rest of dithiosubstituted dimers. Framed in *green*, the orbitals included in the active space employed in the geometry optimizations of the S_1 states

conjunction with the Pople basis set 6-311++G(3df,2p) [13], recommended in previous works for the optimization of species containing sulfur atoms [14–16]. Tables 2, 3, 4, and 5 collect the valence vertical electronic excitation energies and oscillator strengths, calculated with the CASSCF method [17] along with a triple-zeta contracted set of natural orbitals ANO-L (C,O[4s3p2d]/S[5s4p2d]/H[3s2p]) [18]. Other excitations (double or Rydberg transitions) above the highest valence states were not included in the tables for simplicity.

Four active spaces of the sizes (12,14), (12,11), (12,14), and (12,10) were employed to model the UV absorption spectra of HCSSH–HCOOH, HCOSH–HCSOH, HCSOH–HCSOH, and HCOSH–HCOSH. All the above active spaces have in common two lone pairs, $n_{c=x}$ (X=O, S), lying at the dimer plane and sitting at the carbonyl/thiocarbonyl position, and 3 pairs of frontier π orbitals, including a bonding $\left(\pi^1_{c=x}\right)$, a non-bonding $\left(\pi^2_{c=x}\right)$ and an antibonding $\left(\pi^*_{c=x}\right)$ orbital, where in the first two cases the

Table 2 MS-CASPT2 excitation energies Δ*E* (eV, nm), configuration interaction coefficients (CI) and oscillator strengths (*f*), for the valence lower-lying excited states of the HCSSH–HCOOH dimer

State symmetry	MS-CASPT2//CASSCF(12,14)/ANO-L				
	Main configuration	CI coefficient	Δ*E*/eV	Δ*E*/nm	*f*
$1^1A''$ $(S_1)^a$	$n_{c=s} \rightarrow \pi^*_{c=s}$	−0.94	2.79	444	0.4901
$2^1A'$ $(S_2)^a$	$\pi^2_{c=s} \rightarrow \pi^*_{c=s}$	0.91	4.50	276	0.0864
$2^1A''$ $(S_3)^a$	$n_{c=o} \rightarrow \pi^*_{c=o}$	−0.85	5.93	209	0.1802
$3^1A'$ $(S_4)^a$	$\pi^1_{c=s} \rightarrow \pi^*_{c=s}$	0.76	6.84	181	0.1704
	DE	−0.50			
$3^1A''$ $(S_5)^b$	$n_{c=o} \rightarrow \pi^*_{c=s}$	0.87	7.34	169	0.0211
$4^1A''$ $(S_6)^b$	$n_{c=s} \rightarrow \pi^*_{c=o}$	−0.84	7.42	167	0.0006
$4^1A'$ $(S_7)^b$	$\pi^2_{c=o} \rightarrow \pi^*_{c=s}$	−0.71	7.86	158	0.0289
	$\pi^2_{c=o} \rightarrow \pi^*_{c=o}$	−0.55			
$5^1A'$ $(S_8)^a$	$\pi^2_{c=o} \rightarrow \pi^*_{c=o}$	−0.56	8.36	148	0.0000
	$\pi^2_{c=s} \rightarrow \pi^*_{c=o}$	0.53			
	$\pi^2_{c=o} \rightarrow \pi^*_{c=s}$	0.45			
$6^1A'$ $(S_9)^a$	DE	−0.79	8.56	145	0.0009
$7^1A'$ $(S_{10})^b$	$\pi^2_{c=s} \rightarrow \pi^*_{c=o}$	−0.70	9.28	134	0.0002
	$\pi^2_{c=o} \rightarrow \pi^*_{c=o}$	−0.43			
$8^1A'$ $(S_{11})^a$	DE	−0.69	9.46	131	0.0008
	$\pi^1_{c=s} \rightarrow \pi^*_{c=s}$	0.49			
Ground state total energy: −1023.972452 Eh					

DE double excitations

[a] Intramonomer excitations, [b] intermonomer excitations

superindex represents the number of nodes of the corresponding MO, (See Fig. 2).

All the remaining orbitals until completing the final sizes correspond to virtual orbitals included to avoid intruder states. All CASSCF calculations were carried out using the state average formalism, under C_s symmetry constraints, entailing the number of roots necessary for describing all valence excited states, that is, 8 roots of both A′ and A″ symmetries for HCSSH–HCOOH, 6 and 3 roots of A′ and A″ symmetries for HCOSH–HCSOH, 8 and 6 roots of A′ and A″ symmetries for HCSOH–HCSOH, and 5 and 3 roots of A′ and A″ symmetries for HCOSH–HCOSH. Dynamic correlation was incorporated via a second-order perturbation theory treatment of the CASSCF wave function through the MS-CASPT2 method [19]. A real level shift [20] parameter of 0.3 was employed in order to remove further problems connected to intruder states.

Excited state geometry optimizations were performed at the CASSCF/aug-cc-pVTZ [21–23] level of theory, using the (8,6) active space defined in Fig. 2. The same protocol was employed for optimizing the ground states in order to analyze the structural changes undergone by these species

Table 3 MS-CASPT2 excitation energies ΔE (eV, nm), configuration interaction coefficients (CI), and oscillator strengths (f), for the valence lower-lying excited states of the HCOSH–HCSOH dimer

State Symmetry	MS-CASPT2//CASSCF(12,11)/ANO-L				
	Main configuration	CI coefficient	ΔE/eV	ΔE/nm	f
$1^1A''$ (S_1)	$n_{c=s} \rightarrow \pi^*_{c=s}$	−0.94	3.62	343	0.2494
$2^1A''$ (S_2)	$n_{c=o} \rightarrow \pi^*_{c=o}$	−0.91	4.95	251	0.6738
$2^1A'$ (S_3)	$\pi^2_{c=s} \rightarrow \pi^*_{(c=o+c=s)}$	0.74	5.34	232	0.0051
	$\pi^2_{c=s} \rightarrow \pi^*_{(c=o-c=s)}$	−0.48			
$3^1A'$ (S_4)	$\pi^2_{c=o} \rightarrow \pi^*_{(c=o+c=s)}$	−0.71	5.77	215	0.0066
	$\pi^2_{c=o} \rightarrow \pi^*_{(c=o-c=s)}$	−0.47			
$3^1A''$ (S_5)	$n_{c=s} \rightarrow \pi^*_{c=o}$	−0.94	6.28	198	0.0000
$4^1A'$ (S_6)	$\pi^2_{c=s} \rightarrow \pi^*_{(c=o-c=s)}$	−0.70	7.42	167	0.0000
	$\pi^2_{c=s} \rightarrow \pi^*_{(c=o+c=s)}$	−0.55			
$5^1A'$ (S_7)	$\pi^2_{c=o} \rightarrow \pi^*_{(c=o-c=s)}$	−0.70	7.84	158	0.0000
	$\pi^2_{c=o} \rightarrow \pi^*_{(c=o+c=s)}$	0.54			

Ground state total energy:
−1023.966949 Eh

(+) and (−) stand for positive and negative linear combinations of the orbitals of the different dimer moieties

upon electronic excitation. Finally, the bonding in the excited states will be investigated in the frame of the AIM theory of Bader [24], through the mapping of the topology of the electron density and localization of bond and ring critical points.

Ground and excited state geometry optimizations were carried out using Gaussian 09 [25], while vertical energies and oscillator strengths were calculated with MOLCAS 7.4 [26] suite of programs.

3 Results and discussion

3.1 UV vertical excitation energies

Before start discussing the calculated UV vertical absorption energies of di-thiosubstituted dimers, we shall briefly revisit the main characteristics of the electronic spectra of formic acid dimer and its monosubstituted derivatives, analyzed in detail in ref. [27]. For the sake of clarity, a summary of the vertical energies and oscillator strengths for the electronic transitions absorbing below 10 eV for these species has been included in Table 1. The calculated UV spectra of these three species are characterized by an imaginary division line which separates intramonomer transitions, taking place in a single moiety, and intermonomer or CT transitions involving the two constituting monomers.

Table 4 MS-CASPT2 excitation energies ΔE (eV, nm), configuration interaction coefficients (CI) and oscillator strengths (f), for the low-lying excited states of the HCSOH–HCSOH dimer

State symmetry	MS-CASPT2//CASSCF(12,14)/ANO-L				
	Main configuration	CI coefficient	ΔE/eV	ΔE/nm	f
$1^1A''$ (S_1)	$n_{(A-B)} \rightarrow \pi^*_{(A+B)}$	−0.79	3.56	348	0.0119
	$n_{(A+B)} \rightarrow \pi^*_{(A-B)}$	−0.47			
$2^1A''$ (S_2)	$n_{(A-B)} \rightarrow \pi^*_{(A-B)}$	0.70	3.67	337	0.6679
	$n_{(A+B)} \rightarrow \pi^*_{(A+B)}$	0.58			
$2^1A'$ (S_3)	$\pi^2_{(A)} \rightarrow \pi^*_{(A+B)}$	−0.62	5.03	246	0.0109
	$\pi^2_{(B)} \rightarrow \pi^*_{(A-B)}$	0.35			
$3^1A'$ (S_4)	$\pi^2_{(B)} \rightarrow \pi^*_{(A+B)}$	−0.65	5.44	228	0.0009
	$\pi^2_{(A)} \rightarrow \pi^*_{(A-B)}$	0.47			
	$\pi^2_{(B)} \rightarrow \pi^*_{(A-B)}$	0.32			
$3^1A''$ (S_5)	DE		6.01	206	0.0000
$4^1A''$(S_6)	DE		6.19	200	0.0000
$5^1A''$ (S_7)	$n_{(A-B)} \rightarrow \pi^*_{(A-B)}$	0.59	6.90	180	0.0000
	$n_{(A+B)} \rightarrow \pi^*_{(A+B)}$	−0.69			
$6^1A''$ (S_8)	$n_{(A-B)} \rightarrow \pi^*_{(A+B)}$	0.48	7.06	176	0.0000
	$n_{(A+B)} \rightarrow \pi^*_{(A-B)}$	−0.76			
$4^1A'$ (S_9)	DE		7.08	175	0.0000
$5^1A'$ (S_{10})	DE		7.09	175	0.0008
$6^1A'$ (S_{11})	$\pi^2_{(B)} \rightarrow \pi^*_{A+B)}$	0.37	7.21	172	0.0000
	$\pi^2_{(B)} \rightarrow \pi^*_{(A-B)}$	0.66			
$7^1A'$ (S_{12})	$\pi^2_{(A)} \rightarrow \pi^*_{(A+B)}$	0.42	7.36	168	0.0000
	$\pi^2_{(B)} \rightarrow \pi^*_{(A+B)}$	−0.37			
	$\pi^2_{(A)} \rightarrow \pi^*_{(A-B)}$	−0.68			

Ground state total energy:
−1023.974778 Eh

DE double excitations

(A) and (B) denote the two identical dimer moieties. (+) and (−) stand for positive and negative linear combinations of the orbitals of the different dimer moieties

Within both regions, electronic transitions were found to be arranged according the two established patterns: $n\pi^* - n\pi^* - \pi\pi^* - \pi\pi^*$ characteristic of formic acid dimer spectrum and $n\pi^* - \pi\pi^* - n\pi^* - \pi\pi^*$ governing the absorption spectrum of the mono-thiosubstituted dimers. This change of pattern has its origin in a red-shift of the electronic vertical excitation energies which unevenly affects $n\pi^*$ and $\pi\pi^*$ transitions upon sulfur substitution, which was also found to affect the oscillator strengths of these excitations.

Table 5 MS-CASPT2 excitation energies ΔE (eV, nm), configuration interaction coefficients (CI), and oscillator strengths (f), for the low-lying excited states of the HCOSH–HCOSH dimer

State symmetry	MS-CASPT2//CASSCF(12,10)/ANO-L				
	Main configuration	CI coefficient	ΔE/eV	ΔE/nm	f
$1^1A''$ (S_1)	$n_{(B)} \rightarrow \pi^*_{(B)}$	−0.95	4.89	253	0.0000
$2^1A''$ (S_2)	$n_{(A)} \rightarrow \pi^*_{(A)}$	−0.92	4.96	250	0.8380
$2^1A'$ (S_3)	$\pi^2_{(A-B)} \rightarrow \pi^*_{(A+B)}$	−0.73	5.73	216	0.0190
	$\pi^2_{(A+B)} \rightarrow \pi^*_{(A-B)}$	−0.58			
$3^1A'$ (S_4)	$\pi^2_{(A-B)} \rightarrow \pi^*_{(A-B)}$	0.64	6.01	206	0.0000
	$\pi^2_{(A+B)} \rightarrow \pi^*_{(A+B)}$	0.71			
$4^1A'$ (S_5)	$\pi^2_{(A-B)} \rightarrow \pi^*_{(A-B)}$	−0.71	8.06	154	0.0000
	$\pi^2_{(A+B)} \rightarrow \pi^*_{(A+B)}$	0.63			
$5^1A'$ (S_6)	$\pi^2_{(A-B)} \rightarrow \pi^*_{(A+B)}$	0.59	8.08	153	0.0000
	$\pi^2_{(A+B)} \rightarrow \pi^*_{(A-B)}$	−0.74			
$3^1A''$ (S_7)	$n_{(B)} \rightarrow \pi^*_{(A)}$	0.94	8.27	150	0.0001
Ground state total energy: −1023.962576 Eh					

(A) and (B) denote the two identical dimer moieties. (+) and (−) stand for positive and negative linear combinations of the orbitals of the different dimer moieties

3.1.1 HCSSH–HCOOH

The MS-CASPT2//SA-CASSCF vertical absorption energies for HCSSH–HCOOH dimer are collected in Table 2. According to these results, its UV absorption spectrum would consist of a very intense band peaking at 2.8 eV (S_1) followed by three less intense absorptions in the region of 4.5–7 eV (S_2–S_4). The S_1 and S_3 states present an nπ* character and are localized in the thiosubstituted monomer and in the formic acid moiety, respectively, while the S_2 and S_4 have a predominant ππ* nature.

A careful comparison between Tables 1 and 2 reveals that di-thio-substitution within the same monomer breaks the clear division between intra- and intermonomer excitations characteristic of the unsubstituted and monosubstituted dimers. In addition, no clear pattern among nπ* and ππ* transitions is observed in the electronic spectrum summarized in Table 2 in contrast to HCOOH–HCOOH, HCSOH–HCOOH or HCOSH–HCOOH [27].

There are, however, some absorptions common to the electronic spectra of these four species, such as the intramonomer transitions taking place in the common moiety to the four dimers, that is, the HCOOH monomer. Specifically, the $n_{c=o} \rightarrow \pi^*_{c=o}$ and $\pi_{c=o} \rightarrow \pi^*_{c=o}$ excitations, peaking around 6.1 and 8.3 eV for the unsubstituted and monosubstituted dimers [27] (See Table 1), were calculated at 5.93 and 8.36 eV for HCSSH–HCOOH (See Table 2). The small energy differences registered for the above transitions can be either attributed to the use of different basis sets in both works or alternatively to the different chemical environments surrounding the fragment where the excitations occur. Interestingly, the oscillator strength of these transitions is also affected by the introduction of a second sulfur atom in the molecule. Thus, the intensity of the nπ* transition becomes 100 times stronger in the HCSSH–HCOOH dimer, while the ππ* transition goes from being one of the most intense absorptions in HCOOH–HCOOH and its mono-thiosubstituted derivatives to a dark state in HCSSH–HCOOH.

In general, double thio-substitution within the same monomer affects in a larger extent the rest of the transitions. Specifically, intramonomer excitations occurring in the sulfur-substituted monomer and CT transitions shift to lower energies as compared to HCSOH–HCOOH or HCOSH–HCOOH, being this shift slightly larger when the second sulfur substitution takes place in the carbonyl position.

Finally, it is interesting to mention that simultaneous substitution of the hydroxyl and carbonyl oxygens by sulfur in the same monomer greatly stabilize the $\pi^1_{c=s} \rightarrow \pi^*_{c=s}$ transition. As a consequence, while this transition is observed at 6.84 eV for the HCSSH–HCOOH complex, it was not found among the transitions absorbing below 10 eV in formic acid dimer or its mono-thiosubstituted derivatives.

3.1.2 HCOSH–HCSOH

Table 3 summarizes the MS-CASPT2-calculated valence vertical transition energies and relative intensities for formic acid dimer di-thiosubstituted in the carbonyl and the hydroxyl positions of different monomers. The $n_{c=o} \rightarrow \pi^*_{c=s}$ transition is not reported because it was omitted from the calculation due to the huge number of double excitations which precede it and that complicated the perturbation treatment.

Similarly to HCSSH–HCOOH, the electronic absorption spectrum of HCOSH–HCSOH is governed by nπ* intramonomer excitations, which carry the largest oscillator strengths, see Table 3. A closer look to this table reveals that intra- and intermonomer excitations localize into two different regions of the spectrum, reminding unsubstituted and monosubstituted dimers spectra, although in this case, intra- and intermonomer ππ* excitations are difficult to distinguish since the π* orbitals involved in these transitions spread over the whole molecule.

Also for this species, we find some absorptions peaking at the same wavelengths as in the spectra of monosubstituted

derivatives. In particular, this applies to $n_{c=s} \rightarrow \pi^*_{c=s}$ and $n_{c=o} \rightarrow \pi^*_{c=o}$ transitions peaking at 3.62 and 4.95 eV, also present in HCSOH–HCOOH and HCOSH–HCOOH dimers, respectively. This also applies to $\pi\pi^*$ S_3 and S_4 states, which appear red shifted by 0.2 eV, most probably due to the π^* orbital mixing mentioned above. Red-shifts between 1.3 and 2.8 eV were also registered for the transitions S_5–S_7 taking the thiohydroxyl and thiocarbonyl-substituted derivatives as a reference, leading fortuitously to the recovery of the $n\pi^* - n\pi^* - \pi\pi^* - \pi\pi^*$ ordering characteristic of formic acid dimer.

3.1.3 HCSOH–HCSOH

An inspection of Table 4, containing the vertical excitation energies and oscillator strengths for HCSOH–HCSOH, reveals that both the lone pairs and π^* orbitals describing the lower-lying excitations in this dimer appear as linear combinations of the former orbitals sitting on the two monomers, preventing the discrimination between intra-monomer and CT transitions, similarly to what observed for the dimer described in Sect. 3.1.2. Also in this case, the pattern $n\pi^* - n\pi^* - \pi\pi^* - \pi\pi^*$ was found to govern the two regions in which can be divided the spectrum, typically associated to intra- and intermonomer regions. The organization of the transitions according to this pattern is attributed, in this case, to the high symmetry of this dimer, C_{2h}, which leads to the degeneration or near degeneration (recall that all the calculations were performed under C_s symmetry constraints) between pairs of transitions with the same character. The first pairs of $n\pi^*$ and $\pi\pi^*$ transitions peak at ca. 3.6 and 5.4 eV very close

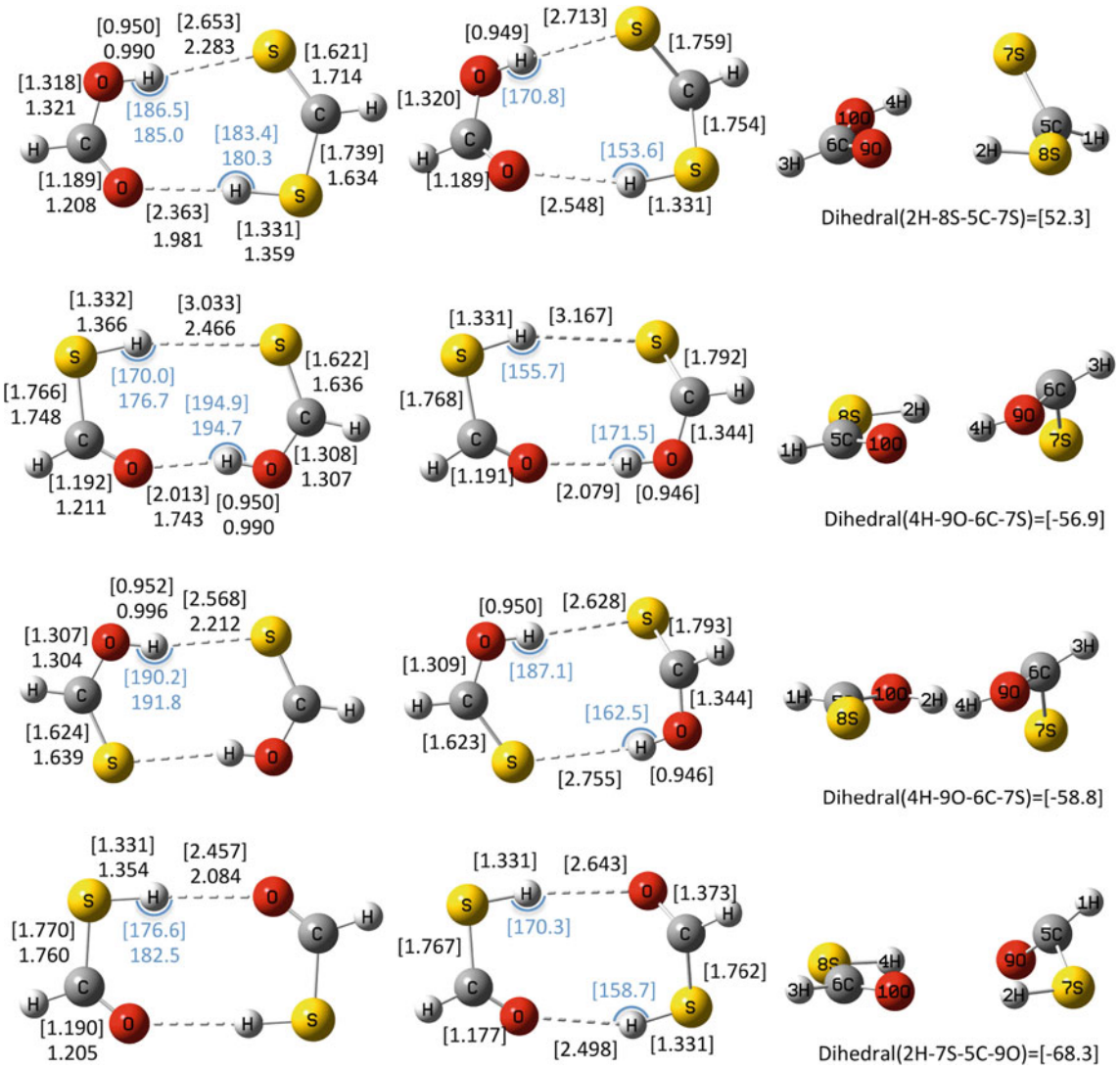

Fig. 3 Optimized geometries for the ground (S_0, first column) and the first excited (S_1, second and third columns) states of di-thiosubstituted derivatives of formic acid dimer. Values in normal font correspond to B3LYP/6-311++G(3df,2p) optimized parameters and CASSCF(8,6)/aug-cc-pVTZ optimized parameters are in *square brackets*. Bond distances are given in Angstrom and angles in degrees

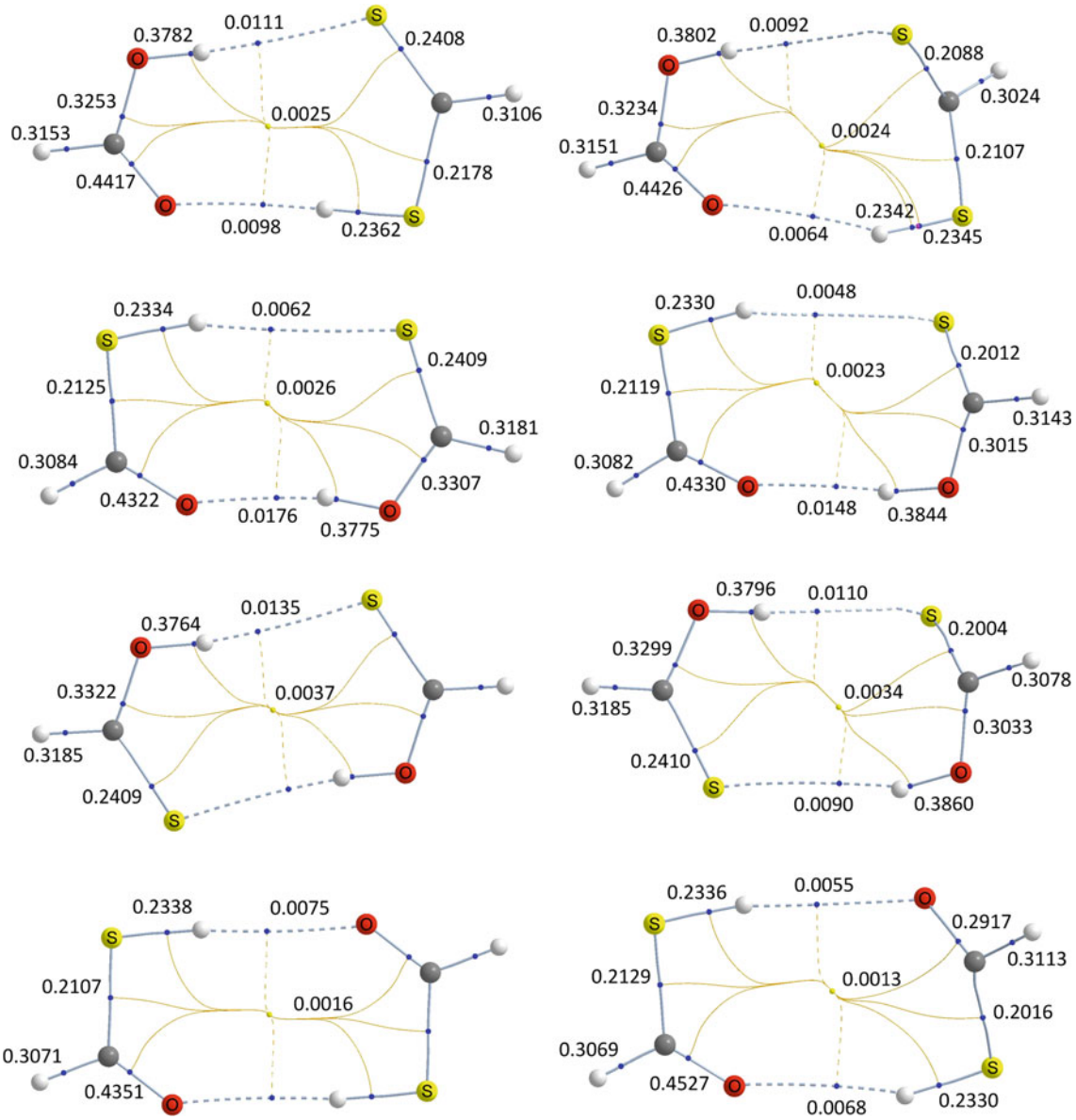

Fig. 4 Molecular graphs for the ground (*left*) and first excited state minima (*right*) of HCSSH–HCOOH, HCOSH–HCSOH, HCSOH–HCSOH, and HCOSH–HCOSH. Electron densities at the BCPs (*blue*) and RCPs (*yellow*) are in a.u

to the wavelengths where the same electronic states absorb in the dimer monosubstituted in the carbonyl position, pointing to the very little influence of the nature of the monomer where the excitation does not take place. As expected, this is not the case of S_7–S_8 $n\pi^*$ and S_{11}–S_{12} $\pi\pi^*$ transitions which experience red-shifts that can amount up to 2.5 eV.

Also interesting, the comparison of the present spectrum with that calculated for the di-thiosubstituted dimer in the hydroxyl and carbonyl position in Table 3 allows establishing the effect of the position of di-thio-substitution—carbonyl or hydroxyl—on the electronic energies. Thus, from the generalized red-shift of the electronic spectrum of HCSOH–HCSOH compared with that of HCOSH–HCSOH, we conclude that a second oxygen-by-sulfur substitution occurring in carbonyl position has a larger effect on the electronic energies.

Introducing a second sulfur atom in carbonyl position has also a great impact in the oscillator strengths and therefore in the shape of the electronic spectrum. In this respect, the intramonomer $\pi\pi^*$ transitions, which were predicted to contribute to the greatest extent to the UV spectrum of the HCSOH–HCOOH dimer, become darker states in this dimer, while the opposite is observed for intramonomer $n\pi^*$ excitations which become the brightest transitions in the di-thiosubstituted monomer.

3.1.4 HCOSH–HCOSH

Finally, this section analyzes the calculated UV absorptions for the di-thiosubstituted dimer in the hydroxyl positions.

This species only differs from the dimer discussed in the previous section, HCSOH–HCSOH, in a double proton transfer, being the former species 3.8 kcal/mol more stable. At 298 K, this process involves an energy barrier of 5.5 kcal/mol that would prevent interconversion between both species.

Due to its C_{2h} symmetry, this dimer shares some of the features already described for the electronic spectrum of the thiosubstituted dimer in both carbonyl positions. As for HCSOH–HCSOH, the lowest lying nπ* and ππ* transitions in this dimer appear grouped in pairs of doubly degenerate excited states absorbing at the same energy as their monosubstituted analog HCOSH–HCOOH, whereas the remaining excitations are shifted to lower energies with respect to the same species. Contrary to the expectations, however, these doubly degenerated transitions do not follow the nπ* − nπ* − ππ* − ππ* sequence observed for the other C_{2h} system. Indeed, the only calculated CT nπ* transition, S_7, (the other was omitted from the multiconfigurational calculations to avoid problems in the perturbation treatment) appears above the least stable ππ* transitions, breaking the pattern.

Finally, the comparison of this spectrum with those of the other two di-thiosubstituted dimers in different monomers allows confirming our conclusions on the larger effect which has the position of thio-substitution on the shift of the electronic energies. In fact, the electronic spectrum for this species is significantly shifted to higher energies than that calculated for the hydroxyl and carbonyl substituted dimer, which in turn is blue shifted compared to that of HCSOH–HCSOH.

Neither the position nor the dimer in which second thiosubstitution occurs seem to have any effect on the oscillator strength since as for the other species studied here the most intense absorption corresponds to an intramonomer nπ* transition.

At this point, it is worth stressing that HCOSH–HCOSH is the only dimer among all the studied not absorbing above 280 nm. This, coupled to the fact that interconversion between HCOSH–HCOSH and HCSOH–HCSOH is not likely to occur, turns this dimer into a potential linker to be used in photovoltaic devices working in the visible/near UV regime.

3.2 Geometries and bonding of the first excited states

Considering that a large change in the geometry of the hydrogen-bonded linker upon excitation might seriously affect the efficiency of the photovoltaic device, hindering the formation of the CT complex, we have optimized the first excited state S_1 of all the dimers. Recall that, according to the results discussed in the previous sections, this state corresponds to the brightest transition in HCSSH–HCOOH and has a non-negligible oscillator strength for HCOSH–HCSOH. Although for the two other dimers, HCSOH–HCSOH and HCOSH–HCOSH, the S_1 does not correspond to the brightest state, due to their symmetry, analogous geometries as the ones optimized here are expected for the states carrying the largest oscillator strengths, that is, S_2, which involve similar excitations.

Figure 3 collects the CASSCF geometries for the ground and first excited states of all the dimers considered in this work. The most remarkable difference between these pairs of structures is the out of plane deviation of the carbonyl/thiocarbonyl group of the monomer where the excitation takes place. This loss of planarity of the molecule is accompanied by a rearrangement of the bond distances and bond angles. Specifically, the population of the π* orbital after the promotion of an electron from the lone pair sitting in the same moiety results in a stretching by 0.01–0.04 Å of the C–XH (X=O, S) bond distance and in a considerably larger elongation of the C=X (X=O, S) bond which in average amounts to 0.17 Å.

This excitation also affects the two HBs that hold together the two monomers, which significantly weaken in the excited state, but has no influence in the geometry of the moiety acting as a spectator during the excitation.

These changes in the geometries lead to a reorganization of the electron density of these species, see Fig. 4. Thus, on going from the S_0 to the S_1, we register an average decrease in the electron density which amounts to 0.037, 0.143, 0.008, and 0.029 e.a.u^{-3} for the C=S, C=O, C–SH, and C–OH bonds, respectively.

These results are useful in providing the trends which should be expected in the geometry changes upon excitation. It is important, however, not to forget the well-known poor performance of CASSCF for the description of hydrogen-bonded structures. Hence, the CASSCF geometries and electron densities of Figs. 3 and 4 are only qualitatively interesting. A quantitatively meaningful description requires a method capable of accurately characterizing excited states and at the same time including dynamic correlation.

4 Concluding remarks

This paper reports on the calculated valence excited states of the four di-thiosubstituted formic acid dimer derivatives which differ in the position (carbonyl and hydroxyl) and subunit which occupy the two sulfur atoms.

Due to the dimeric structure of these species, their absorption spectrum can be divided in two regions,

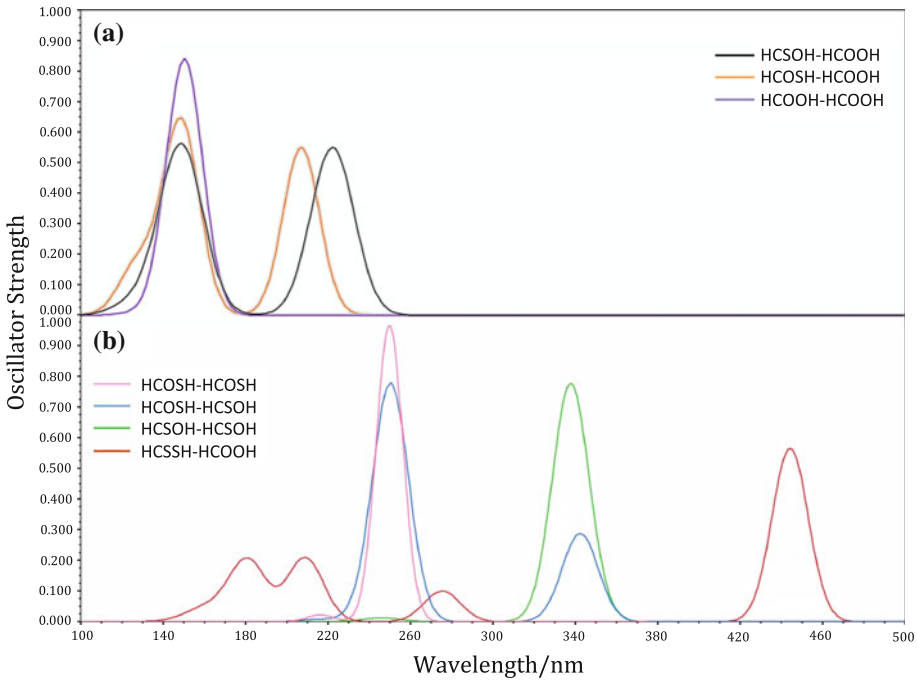

Fig. 5 **a** Simulated absorption spectra based on MS-CASPT2 vertical excitation energies and oscillator strengths for HCOOH–HCOOH (*purple line*), HCOSH–HCOOH (*orange line*), HCSOH–HCOOH (*black line*) (ref. [27]). **b** Simulated absorption spectra based on MS-CASPT2 vertical excitation energies and oscillator strengths for HCOSH–HCOSH (*pink line*), HCOSH–HCSOH (*light blue line*), HCSOH–HCSOH (*green line*), and HCSSH–HCOOH (*red line*)

typically ascribed to intra- and intermonomer or charge transfer absorptions. Except in the case of HCSSH–HCOOH where intra- and intermonomer transitions appear mixed, for the rest of the dimers excited states appear organized into two different regions of the spectrum, separated by an energy gap comprised between ca. 0.5 and 2.0 eV.

Interestingly, all the dimers studied here present one or several nπ* and ππ* excitations peaking at the same wavelength as in the mono-substituted dimers with which they share the moiety where the excitation takes place.

This evidences the very little effect the electronic structure of the monomer acting as a spectator has in the intramonomer transitions. Obviously, this does not hold for the highest lying nπ* and ππ* states, typically of CT character, where the nature of the two moieties involved in the excitations determines the position of the absorption. In general, the above transitions shift further to the red upon introducing a second sulfur atom, especially if the second thio-substitution takes place in the carbonyl position. This is consistent with the fact that the calculated transitions for HCSOH–HCSOH appear at lower energies compared with HCOSH–HCSOH, whose spectrum is in turn red-shifted with respect to HCOSH–HCOSH. Finally, these shifts, which affect irregularly the different electronic transitions, lead to the organization of the nπ* and ππ* according to different patterns. Thus, an nπ* − nπ* − ππ* − ππ* pattern similar to the one found for formic acid dimer was registered for HCOSH–HCSOH, HCSOH–HCSOH, and the lowest energy region of the HCOSH–HCOSH spectrum. In contrast, no apparent ordering among the nπ* and ππ* electronic transitions was found in HCSSH–HCOOH, and an unexpected pattern was observed for the highest energy region of the HCOSH–HCOSH spectrum, where ππ* excitations appear slightly stabilized with respect to the nπ* transition.

Similarly to formic acid dimer and its mono-thiosubstituted derivatives, theory predicts transitions absorbing in the lower energy segment in which can be divided the spectrum to contribute to a larger extent to the UV absorption spectrum. However, whereas in the case of formic acid dimer and its mono-thiosubstituted derivatives, the largest oscillator strength is calculated for ππ* excitations, introducing a second sulfur atom in the molecule renders these transitions dark and augments significantly the intensity of the nπ* transitions which dominate the spectrum of di-thiosubstituted derivatives.

In sum, except for HCOSH–HCOSH which is transparent in the visible, UVA and UVB regions, caution should be exercised when using the remaining dithiosubstituted dimers as hydrogen-bonded linkers in photovoltaic devices with chromophores absorbing above 280 nm, see Fig. 5. Moreover, the corresponding electronic excitations could lead to the out of plane displacement of the carbonyl/thiocarbonyl moiety where the excitation takes place, potentially compromising the formation of the charge transfer complex.

Acknowledgments This work has been partially supported by the DGI Projects No. CTQ2009-13129, by the Project MADRISOLAR2, Ref.: S2009PPQ/1533 of the Comunidad Autónoma de Madrid, and by Consolider on Molecular Nanoscience CSC2007-00010. A generous allocation of computing time at the CCC of the UAM is also

acknowledged. R.V. and A.C. gratefully acknowledge financial support from the Erasmus Mundus Programe (FPA 2010-0147) and a Ciência 2008 contract from FCT (Lisbon, Portugal), respectively.

References

1. Balzani V, Credi A, Venturi M (2008) Chemsuschem 1:26
2. D'Souza F, Ito O (2012) Chem Soc Rev 41:86
3. Beckers EHA, Chen Z, Meskers SCJ, Jonkheijm P, Schenning APHJ, Li X-Q, Osswald P, Wuerthner F, Janssen RAJJ (2006) Phys Chem B 110:16967
4. Sanchez L, Sierra M, Martin N, Myles AJ, Dale TJ, Rebek J, Seitz W, Guldi DM (2006) Angew Chem Int Ed 45:4637
5. Deibel C, Strobel T, Dyakonov V (2010) Adv Mater 22:4097
6. Fuoss M, Accascina F (1959) Electrolytic conductance. Interscience, New York
7. Sreearunothai P, Morteani AC, Avilov I, Cornil J, Beljonne D, Friend RH, Phillips RT, Silva C, Herz LM (2006) Phys Rev Lett 96:117403
8. Segura M, Sanchez L, de Mendoza J, Martin N, Guldi DMJ (2003) Am Chem Soc 125:15093
9. Sessler JL, Wang B, Harriman AJ (1993) Am Chem Soc 115:10418
10. Yu M-L, Wang S-M, Feng K, Khoury T, Crossley MJ, Fan Y, Zhang J-P, Tung C-H, Wu L-ZJ (2011) Phys Chem C 115:23634
11. Becke ADJ (1993) Chem Phys 98:5648
12. Lee CT, Yang WT, Parr RG (1988) Phys Rev B 37:785
13. Hehre WJ, Radom L, Schleyer PvR, Pople JA (1986) Ab initio molecular orbital theory. Wiley Interscience, New York
14. Jonas V, Frenking G (1991) Chem Phys Lett 177:175
15. Timoshkin A, Frenking GJ (2000) Chem Phys 113:8430
16. González L, Mó O, Yáñez M (1996) Chem Phys Lett 263:407
17. Roos BO, Taylor PR, Siegbahn PEM (1980) Chem Phys 48:157
18. Widmark PO, Malmqvist PÅ, Roos BO (1990) Theor Chim Acta 77:291
19. Finley J, Malmqvist PA, Roos BO, Serrano-Andres L (1998) Chem Phys Lett 288:299
20. Roos BO, Andersson K (1995) Chem Phys Lett 245:215
21. Woon DE, Dunning TH Jr (1993) J Chem Phys 98:1358
22. Dunning TH Jr (1007) J Chem Phys 1989:90
23. Kendall RA, Dunning TH Jr, Harrison RJJ (1992) Chem Phys 96:6796
24. Bader RFW (1990) Atoms in molecules: a quantum theory. Clarendon Press, Oxford
25. Frisch MJ et al (2009) Gaussian 09, Revision A.1. Gaussian, Inc., Wallingford
26. Aquilante F et al (2010) J Comput Chem 31:224
27. Cimas A, Mó O, Yáñez M, Martin N, Corral I (2010) Phys Chem Chem Phys 12:13037